Volume 17
Number 18
13 May 2026
Pages 8809–9312

Chemical Science

rsc.li/chemical-science

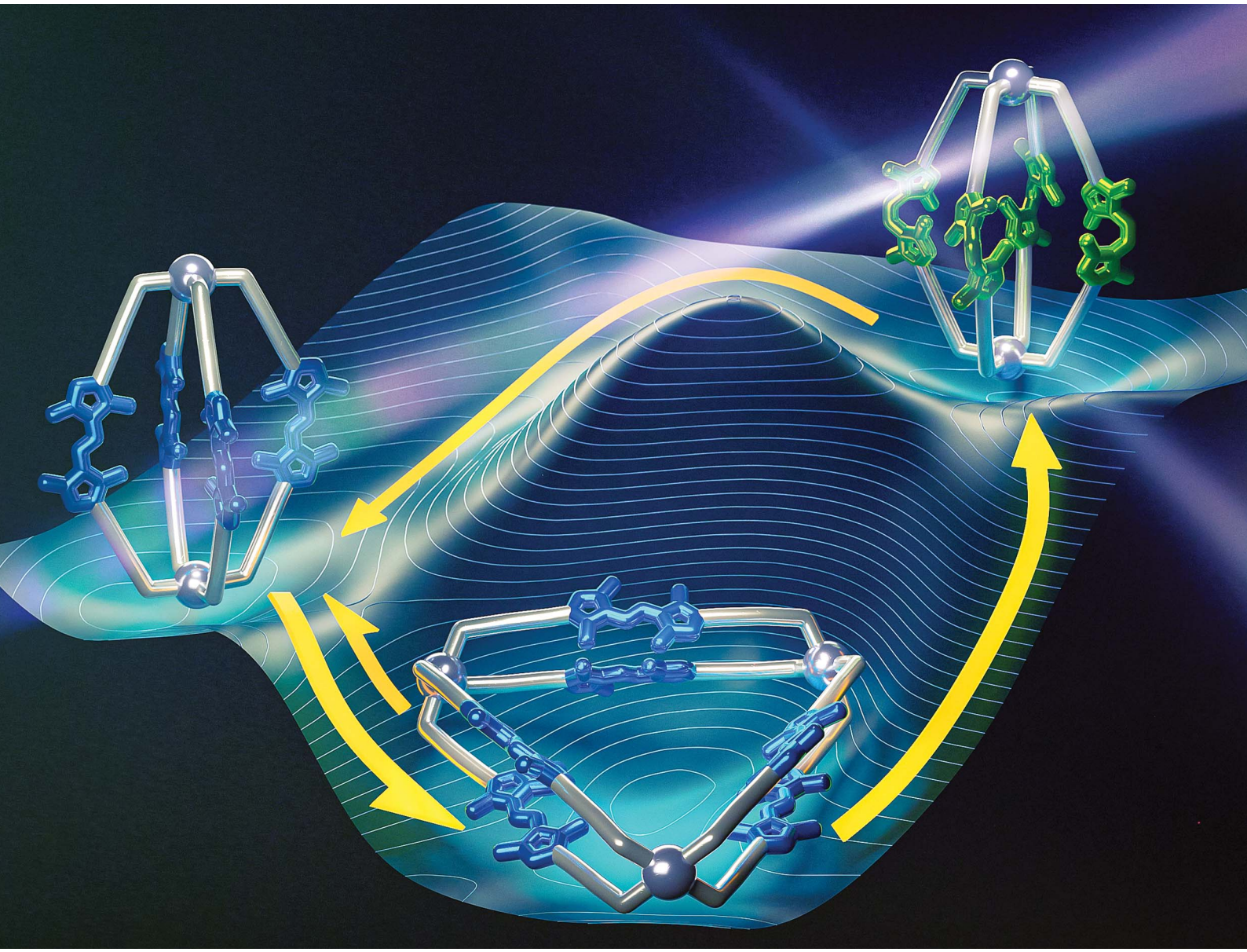

ISSN 2041-6539

ROYAL SOCIETY OF CHEMISTRY

EDGE ARTICLE
Larissa K. S. von Krbek *et al.*
White-light powered autonomous molecular ratchet drives Pd^{II} capsules out of equilibrium

Chemical Science

ROYAL SOCIETY OF CHEMISTRY

EDGE ARTICLE

View Article Online
View Journal | View Issue

Cite this: *Chem. Sci.*, 2026, **17**, 8959

All publication charges for this article have been paid for by the Royal Society of Chemistry

Received 3rd December 2025
Accepted 20th April 2026

DOI: 10.1039/d5sc09472k

rsc.li/chemical-science

White-light powered autonomous molecular ratchet drives Pd^{II} capsules out of equilibrium

Lidón Pruñonosa Lara, [a] Benedikt Bädorf, [b] Maximilian J. Notheis, [a] Gregor Schnakenburg, [c] Stefan Grimme [b] and Larissa K. S. von Krbek *[a]

Using an energy source to drive chemical reactions away from equilibrium is essential for life and remains a significant challenge in designing artificial out-of-equilibrium nanosystems and molecular machines. Achieving autonomous operation of such systems, as observed in nature, presents an even greater difficulty. Here, we report Pd^{II}-mediated coordination capsules based on ligand **1** embedding an azobispyrazole photoswitch. The more thermodynamically stable *E*-photoisomer forms an equilibrium mixture of a Pd^{II}_3(*E*-**1**)$_6$ double-walled triangle and a Pd^{II}_2(*E*-**1**)$_4$ lantern in a 78 : 22 ratio. UV-light irradiation transforms both structures into a Pd^{II}_2(*Z*-**1**)$_4$ lantern, which then reverts solely to the out-of-equilibrium Pd^{II}_2(*E*-**1**)$_4$ lantern when exposed to visible light. The complete photoisomerisation proceeds through an information ratchet mechanism that can operate autonomously under continuous white light or sunlight exposure, selectively accumulating the out-of-equilibrium Pd^{II}_2(*E*-**1**)$_4$ structure. This work demonstrates how autonomous, light-driven processes can be harnessed to direct non-equilibrium behaviour in complex coordination assemblies.

Introduction

Driving chemical systems away from equilibrium and harnessing endergonic reactions are essential for powering molecular machinery and developing adaptive materials.[1–4] Molecular ratchets can drive systems out of equilibrium at a molecular level.[1,3–8] Just as a mechanical ratchet allows movement in only one direction, a molecular ratchet is a chemical reaction cycle, in which the components react preferentially in a single direction due to a kinetic bias.[1,2,9] If this unidirectionality results from transition-state energy (or rate) differences, where one intermediate along the reaction pathway reacts more quickly than another, the ratchet is known as an information ratchet.[1–4,10–14] In contrast, an energy ratchet[15–17] relies on statistically-driven thermodynamic relaxation between intermediates in a kinetically defined region in the reaction cycle to determine its directionality.[1–4] Operating molecular ratchets autonomously, like most natural processes, still presents a significant challenge.[1,18,19] When operating molecular ratchets, light acts as an advantageous stimulus for *in situ* control, allowing precise spatial and temporal regulation without producing unwanted side products.[20,21] Additionally, it can be tuned to a specific wavelength, which activates both forward and reverse reactions, potentially enabling autonomous operation of information and energy ratchets alike.[1]

Harnessing light in molecular ratchets requires integrating photoswitches, such as azobenzenes,[22–27] diazocines,[28–30] crowded alkenes,[31,32] imines[33,34] or dithienylethanes (DTE)[35–38] into the system components. Aligning multiple switches inside a self-assembled supramolecular organic or metal–organic capsule can amplify the switching effect. Despite this advantage, examples of molecular ratchets and out-of-equilibrium structures in supramolecular capsules are still scarce.[1,24,28–30,39] Beves and coworkers[40] demonstrated, that light can be used to disturb the equilibrium between a Pd_3L_6 triangle and a Pd_4L_8 tetrahedron, increasing the amount of the out-of-equilibrium structure to 82%. Feringa, Kathan, and colleagues[24] described a supramolecular organic capsule that acts as a molecular ratchet, leveraging photoisomerisation and imine exchange to create an out-of-equilibrium open capsule. In previous work,[30] we demonstrated how a diazocine-containing, triple-stranded bimetallic helicate can autonomously operate as a molecular energy ratchet, furthermore using this mechanism to accelerate regioselective metal cation exchange within the structure.

Here, we describe the formation of metallo-supramolecular capsules from a bispyridine ligand **1** with an azobispyrazole[41–45] backbone (Scheme 1). Azo-bispyrazoles are photoswitches derived from azobenzene and arylazopyrazole, which have been scarcely explored in supramolecular systems. The ligand exhibits outstanding photophysical properties, with near-quantitative $E \rightarrow Z$ and $Z \rightarrow E$ conversions and no appreciable photobleaching. Moreover, the pyrazole units offer conformational flexibility, enabling the *E*-configuration of the

[a]*Kekulé-Institut für Organische Chemie und Biochemie, Rheinische Friedrich-Wilhelms-Universität Bonn, Gerhard-Domagk-Str. 1, 53121 Bonn, Germany. E-mail: larissa.vonkrbek@uni-bonn.de*

[b]*Mulliken Center for Theoretical Chemistry, Clausius Institute for Physical and Theoretical Chemistry, University of Bonn, Beringstr. 4, 53115 Bonn, Germany*

[c]*Institut für Anorganische Chemie, Rheinische Friedrich-Wilhelms-Universität Bonn, Gerhard-Domagk-Str. 1, 53121, Bonn, Germany*

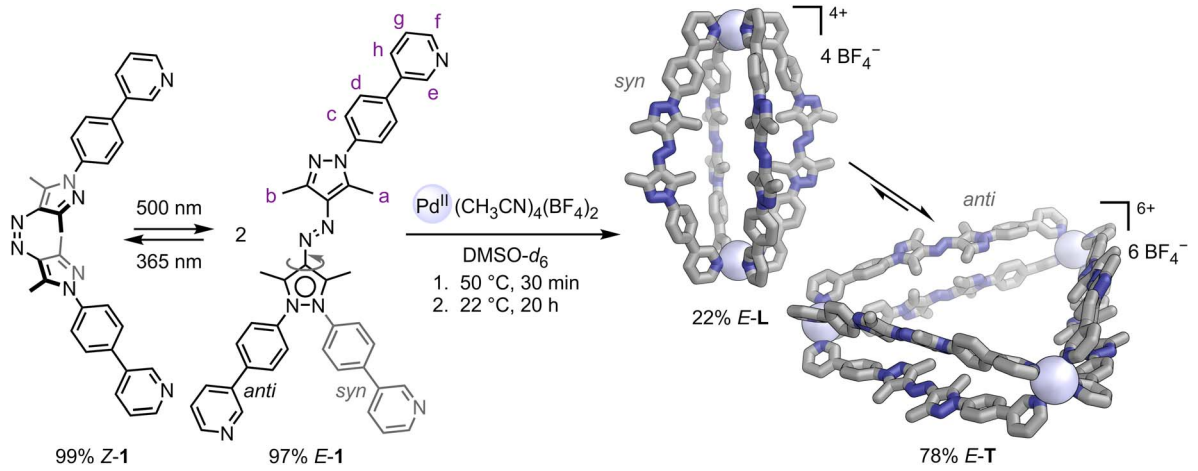

Scheme 1 Left: photoswitching between the two isomers of **1**. Ligand *E*-**1** exhibits two distinct conformations: *syn* and *anti*. Right: self-assembly of ligand *E*-**1** and Pd(CH$_3$CN)$_4$(BF$_4$)$_2$ yielding 22% lantern *E*-**L** (containing *syn*-*E*-**1**; single crystal X-ray structure shown) and 78% triangle *E*-**T** (containing *anti*-*E*-**1**; GFN2-xTB [ALPB: DMSO][46,47],† structure shown). Hydrogens and counterions omitted for clarity; C: grey, N: blue, Pd^{II}: blue white.

ligand to self-assemble both into a Pd$^{II}_3$(*E*-**1**)$_6$ double-walled triangle and a Pd$^{II}_2$(*E*-**1**)$_4$ lantern structure in the presence of Pd^{II} ions. Photoswitching and subsequent capsule rearrangement represent a molecular ratchet that drives the system away from thermodynamic equilibrium by exploiting the kinetic asymmetry of the reaction cycle, resulting in nearly quantitative conversion to the out-of-equilibrium structure, *i.e.* the Pd$^{II}_2$(*E*-**1**)$_4$ lantern. We elucidated the complex ratchet mechanism experimentally and through quantum chemistry-based calculations, regarding its thermodynamics and kinetics. Crucially, continuous white-light or sunlight irradiation operates the molecular ratchet autonomously, with the constant $E \rightarrow Z$ and $Z \rightarrow E$ photoisomerisations driving an information ratchet mechanism, enriching the mixture with the out-of-equilibrium Pd$^{II}_2$(*E*-**1**)$_4$ lantern. Our system exemplifies a rare autonomous, light-powered molecular ratchet within a supramolecular structure: it exhibits directional behaviour under constant illumination, continuously pushing the system out of equilibrium without requiring alternating stimuli. This system could advance the development of autonomous molecular ratchets, serving as an initial step toward harnessing out-of-equilibrium systems for light-driven reaction cascades or molecular machines.

Results and discussion

Synthesis and photoswitching of ligand 1

Photoswitchable azobispyrazole-containing ligand **1** was synthesised by Chan–Lam coupling between (4-(pyridin-3-yl) phenyl)boronic acid and azobispyrazole photoswitch (*E*)-1,2-bis(3,5-dimethyl-1*H*-pyrazol-4-yl)diazene (**S4**; SI Fig. S1 and Section S2.5).

At ambient conditions, ligand **1** predominantly exists in its thermodynamically more stable *E*-configuration (85% *E*-**1**). This is supported by the DFT-computed free energy difference† between *E*-**1** and *Z*-**1** of $\Delta G = +47.4$ kJ mol^{-1} in favour of *E*-**1** (SI, Section S8.2). Single crystals of ligand *E*-**1** were grown by slow evaporation of solvent from a CD_2Cl_2 solution of **1**. The X-ray crystal structure shows the expected *E*-configuration of the N=N double bond (SI, Section S7).

Irradiation of **1** with 365 nm light causes $E \rightarrow Z$ isomerisation, reaching a photostationary state (PSS) of 99% *Z*-**1** (CD_2Cl_2, Scheme 1, left; SI, Section S4.2). This process can be reversed either by exposing *Z*-**1** to 500 nm light (97% *E*-**1**) or through thermal relaxation, which has a half-life of $\tau_{\frac{1}{2}} = 10$ h at 60 °C in DMF (SI, Fig. S59). The photoswitching of ligand **1** is rapid and fully reversible, usually requiring less than 1 minute of irradiation in either direction (24 μM in DMF, 0.2 mW light power), with no appreciable photobleaching over ten switching cycles (SI, Fig. S57, right). Notably, the photostationary states of ligand **1** were quite similar to those of the parent photoswitch **S4**. However, ligand **1** exhibited a significant increase in thermal half-life. This suggests that the 4-(pyridin-3-yl)phenyl substitution did not hinder photoswitching. The substitution of other azo-based photoswitches is known to impede photoswitching.[48]

Synthesis of Pd^{II} capsules

Mixing ligand **1** with Pd(CH$_3$CN)$_4$(BF$_4$)$_2$ in a 2 : 1 stoichiometric ratio in deuterated dimethyl sulfoxide (DMSO-d_6) at 50 °C yielded two Pd^{II} complexes after 30 minutes: a Pd$^{II}_3$(*E*-**1**)$_6$ double-walled triangle *E*-**T** and a Pd$^{II}_2$(*E*-**1**)$_4$ lantern *E*-**L** (Scheme 1). Triangle *E*-**T** and lantern *E*-**L** equilibrated to a 78 : 22 ratio at 22 °C over 20 hours (SI, Fig. S43), and the mixture was characterised using single-crystal X-ray diffraction, mass spectrometry, ^{1}H NMR, and UV-vis spectroscopy (Fig. 1; SI, Sections S2.6 and S7).

The pyrazole groups in ligand **1** can adopt either an *anti* or *syn* orientation, with protons H-*a* and H-*b* positioned on opposite sides of the *azo* bridge or on the same side. This conformational shift from *anti* to *syn* results in a change in the angle between the pyridine nitrogens' coordination vectors: 60° for *anti* and 0° for *syn*. This notable conformational flexibility in ligand **1** enables the formation of both triangle *E*-**T** and lantern *E*-**L** from the same ligand, despite the vastly different angles

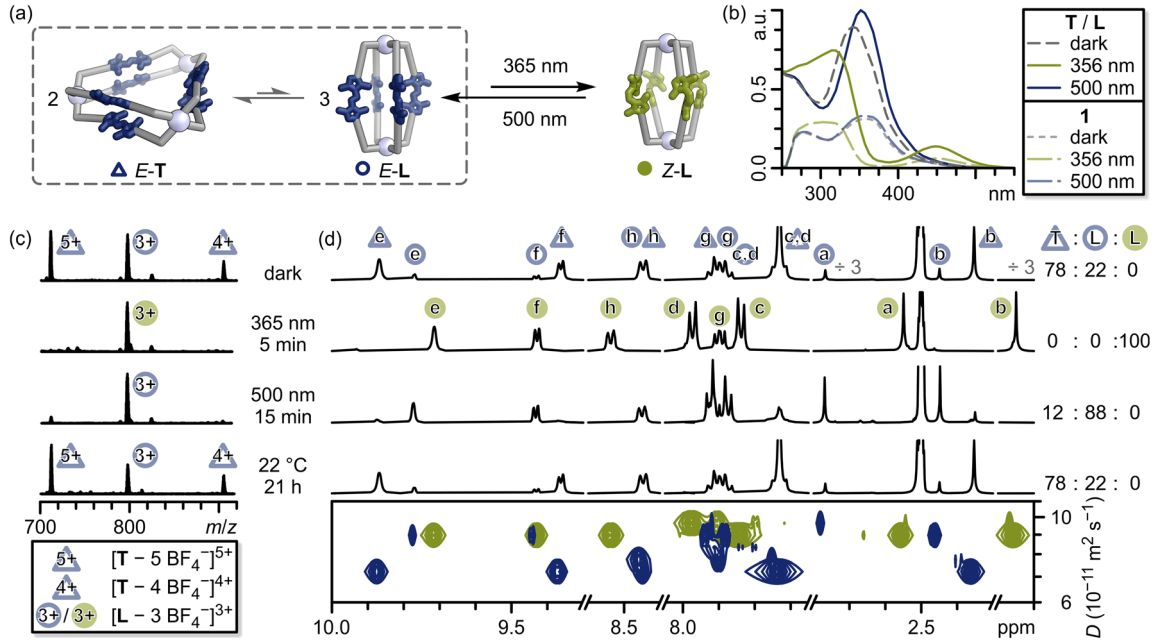

Fig. 1 (a) The triangle *E*-**T**/lantern *E*-**L** mixture converts to lantern *Z*-**L** upon irradiation with 365 nm light. Irradiation of lantern *Z*-**L** with 500 nm light reverts it to *E*-**L**, exclusively, which then equilibrates back to the original triangle *E*-**T**/lantern *E*-**L** ratio over time. (b) Normalised UV-vis spectra of the triangle *E*-**T**/lantern *E*-**L** mixture and ligand **1** (DMSO) before and after irradiation with 365 nm and 500 nm light for 1 min, respectively. Spectra of *E*-**T**/*E*-**L** and **1** are normalised to 1.0 and 0.375, respectively, for clarity. (c and d) Triangle *E*-**T**/lantern *E*-**L** mixture before and after irradiation with 365 nm and 500 nm light for 1 min, respectively, as well as after equilibration under light exclusion at 22 °C for at least 21 h (top to bottom) monitored by (c) ESI mass spectrometry (DMSO/CH_3CN) and (d) ^{1}H NMR spectroscopy (700 MHz, DMSO-d_6, 298 K), including ^{1}H DOSY NMR of the triangle *E*-**T**/lantern *E*-**L** mixture before and after irradiation with 365 nm light (blue and green, respectively). Note that proton H-*a* of triangle *E*-**T** is below the DMSO solvent signal, but can be observed by VT NMR (SI, Fig. S46).

required[49–52] between the pyridine nitrogens' coordination vectors. We could confirm the anti-conformation of the ligands in triangle *E*-**T** using one-dimensional ^{1}H ROESY NMR, based on contacts between protons H-*a* and H-*b*, which are absent in lantern *E*-**L**, in line with the expected *syn*-conformation of the ligands in *E*-**L** (SI, Section S2.6).

Lantern *E*-**L** crystallised in the triclinic space group $P\bar{1}$ (Scheme 1; SI, Section S7). Four ligands **1** connect two Pd^{II} centres, with the crystallographic inversion centre located in the centre of the capsule. The pyrazole groups in ligand **1** display the expected *syn*-orientation, with protons H-*a* and H-*b* on opposite sides of the azo bridge, enabling the pyridine units to have a 0° angle between their coordination vectors, which is essential for lantern formation (SI, Section S2.6). This *syn*-ligand conformation is not C_2 symmetric; therefore, the ligands can be oriented either pointing "up" or "down" within the lantern structure (SI, Fig. S13).‡ The X-ray crystal structure shows two ligands pointing upwards and two pointing downwards in a *cis*-arrangement of the two ligand orientations, with the centre of the lantern being a centre of inversion. In theory, three additional isomers would be possible: a *trans*-arrangement of the two ligands pointing upwards and downwards, three ligands pointing up and one pointing down, or all ligands pointing in the same direction (SI, Fig. S13). A large number of possible isomers were computationally modelled, revealing only low relative energy differences of 6.3 kJ mol $^{-1}$ or less between these isomers (SI, Section S8.4), which suggests that lantern *E*-**L** might exist in different isomers in solution. The azo groups probably rotate within lantern *E*-**L** causing interconversion between its isomers, as has been observed in other azobenzene-containing structures.[53–55] Our computationally predicted structure, with the ligands arranged in a *cis*-configuration, shows excellent agreement with the X-ray crystal structure, validating the computational approach† (Fig. 2; SI, Section S8.5).

The high-resolution electrospray ionisation (ESI) mass spectrum of the 78 : 22 triangle *E*-**T**/lantern *E*-**L** mixture under light exclusion displayed two series of signals corresponding to the species $[\mathbf{T}{-}n(BF_4)]^{n+}$ (n = 3, 4, 5, 6) and $[\mathbf{L}{-}n(BF_4)]^{n+}$ (n = 2, 3, 4; Fig. 1c, top; SI, Fig. S24), respectively. The ^{1}H NMR spectrum exhibited two sets of ligand signals in a 78 : 22 ratio (Fig. 1d, top). The number of signals related to the major and minor components is consistent with one-half of one ligand environment being unique, meaning all ligands are identical and have twofold symmetry. This fits well with a triangle and a lantern structure coexisting in solution. Note that some very minor species were also observed, which we tentatively assign to other possible isomers of lantern *E*-**L** (see above and SI Section S8.4).

UV-vis revealed a strong $\pi \rightarrow \pi^*$ absorption band at $\lambda_{\pi\rightarrow\pi^*}$ = 335 nm, reminiscent of the $n \rightarrow \pi^*$ absorption band in free ligand *E*-**1** ($\lambda_{n\rightarrow\pi^*}$ = 350 nm), indicating that all ligands are in their *E*-configurations in both metallo-supramolecular structures (Fig. 1b). ^{1}H DOSY NMR revealed, that the two species have clearly distinguishable diffusion coefficients ($D_{E\text{-}\mathbf{T}} = 7.3 \times 10^{-11}$ and $D_{E\text{-}\mathbf{L}} = 9.1 \times 10^{-11}$ m^2 s^{-1}) corresponding to the major and minor species in ^{1}H NMR, respectively. This allowed us to identify the major species as triangle *E*-**T** and the minor species as lantern *E*-**L**. The solvodynamic diameters of $d_{E\text{-}\mathbf{T}}$ =

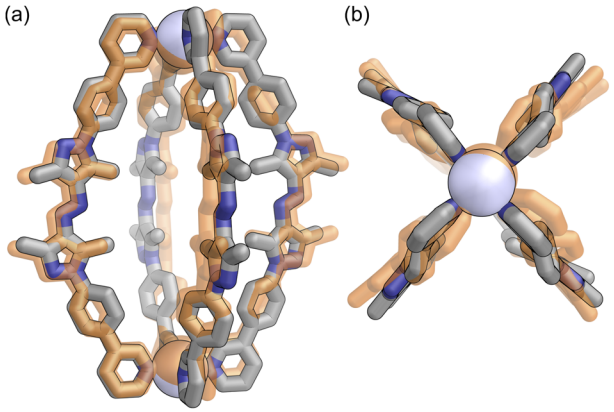

Fig. 2 Overlay of the experimental structure of lantern *E*-L (orange) with the computationally obtained structure† ((a) side view, (b) top view; C: grey, N: blue, Pd^{II}: blue white) from a CREST[56] conformational search, reoptimized at the ωB97X-3c [CPCM: DMSO] level of theory.[57] The structures have a permutation-invariant root-mean-square deviation (iRMSD)[58] of 1.1 Å.

27.8 Å and $d_{E\text{-}\mathbf{L}} = 22.4$ Å align well with the dimensions of the computational structure of triangle *E*-**T** and the X-ray crystal structure of lantern *E*-**L** ($d_{E\text{-}\mathbf{T}} = 25.2$ Å and $d_{E\text{-}\mathbf{L}} = 19.8$ Å, respectively; SI, Fig. S23). UV-vis, NMR, and ESI MS data are consistent with the coexistence of a double-walled triangle *E*-**T** and a lantern *E*-**L**.

Due to the lability of the Pd^{II}–pyridine bonds, triangle *E*-**T** and lantern *E*-**L** exist in a dynamic equilibrium. As expected for an equilibrium between a larger and a smaller species, entropically favoured lantern *E*-**L** could be enriched in the mixture by diluting the complex mixture solution (SI, Section S3.3). At ligand concentrations below 7.0 mM, signals of free ligand *E*-**1** began to appear, which is why all studies on the triangle *E*-**T**/lantern *E*-**L** mixture were conducted at a ligand concentration between 7.5–8.5 mM. Similarly, increasing the temperature of the triangle *E*-**T**/lantern *E*-**L** mixture shifted the equilibrium towards the entropically favoured lantern *E*-**L** (SI, Section S3.4). Van't Hoff analysis showed that the enthalpic and entropic contributions of the 3 *E*-**L** ⇌ 2 *E*-**T** equilibrium are $\Delta H = -50.6 \pm 7.7$ kJ mol^{-1} and $\Delta S = -76.3 \pm 29.9$ J K^{-1} mol^{-1}, respectively. These values correspond to a Gibbs free energy difference of $\Delta G = -27.8 \pm 13.0$ kJ mol^{-1}, consistent with a higher thermodynamic stability of triangle *E*-**T**, and an equilibrium constant of $K = 76\,000 \pm 36\,000$ M^{-1} at 298 K.

Photoswitching of Pd^{II} capsules

Irradiation of the 78 : 22 triangle *E*-**T**/lantern *E*-**L** mixture in DMSO-d_6 with 365 nm light produced a single component: a lantern with all ligands in their *Z*-configurations, namely *Z*-**L**, which was characterised by mass spectrometry, NMR, and UV-vis spectroscopy (Fig. 1; SI Section S2.7). In ^{1}H NMR, the proton signals of triangle *E*-**T** and lantern *E*-**L** completely disappeared after irradiation with 365 nm light, and a new set of signals appeared, consistent with one half of one ligand environment being unique (Fig. 1d, second from top). This suggests all ligands are identical and possess twofold symmetry, which would align with a lantern-shaped structure. Protons H-*a* and H-*b* were high-field shifted by 0.22 and 1.09 ppm, respectively, when comparing lanterns *E*-**L** and *Z*-**L**, indicating H-b to feel the anisotropy of the neighbouring pyrazole ring, which would be expected, if the ligands were in their *Z*-configurations (compare SI, Fig. S51 and S55). Additionally, ROESY contacts between protons H-*a* and H-*b* align with the *Z*-configurations of ligands in *Z*-**L** (SI, Fig. S30). UV-vis spectra after 365 nm irradiation showed a less intense and blue-shifted π → π* absorption band ($\lambda_{\pi\rightarrow\pi^*} = 310$ nm), along with a new *n*→π* absorption band ($\lambda_{n\rightarrow\pi^*} = 435$ nm), which resembles the UV-vis spectrum of ligand **1** in its *Z*-configuration (Fig. 1b). This further supports that the ligands in lantern *Z*-**L** are all in their *Z*-states. High-resolution ESI mass spectrometry revealed a series of signals corresponding to the species $[\mathbf{L}-n(BF_4)]^{n+}$ ($n = 2$, 3, 4), indicating the presence of a lantern-shaped capsule (Fig. 1c, second from top). ^{1}H DOSY NMR revealed a diffusion coefficient similar to that of lantern *E*-**L**, indicating a comparable solvodynamic diameter of $d_{Z\text{-}\mathbf{L}} = 21.8$ Å, suggesting the presence of a lantern-shaped capsule in solution as well. Hence, we conclude that 365 nm light irradiation of the triangle *E*-**T**/lantern *E*-**L** mixture converts the structures to lantern *Z*-**L**.

Besides the main species observed in the ^{1}H NMR spectrum of *Z*-**L**, several sets of minor signals could be observed (SI, Fig. S27), which are significantly more pronounced than in lantern *E*-**L** (compare SI, Fig. S15). Since the ESI mass spectrum of lantern *Z*-**L** indicates clean formation of lantern *Z*-**L** and ligand **1** is chiral in its *Z*-configuration, we tentatively assume these minor signals are caused by the four additional possible diastereomers of lantern *Z*-**L**.§ We calculated† all possible diastereomers and obtained only minor differences in their free energies (approx. 5.0 kJ mol^{-1} or less), which supports our hypothesis (SI, Section S8.3).

Lantern *Z*-**L** demonstrates good thermodynamic stability with a thermal half-life of $\tau_{\frac{1}{2}} = 21$ min at 75 °C in DMSO, as determined by ^{1}H NMR spectroscopy. At room temperature, thermal relaxation takes approximately one year to complete (SI, Fig. S73). Over that period, several distinguishable intermediates were observed. We tentatively assume these to be the four possible intermediates: *Z*,*Z*,*Z*,*E*-**L**, *cis*- and *trans*-*Z*,*Z*,*E*,*E*-**L**, and *Z*,*E*,*E*,*E*-**L**. These intermediates might occur during the stepwise thermal relaxation of the four ligands from *Z*,*Z*,*Z*,*Z*-**L** to *E*,*E*,*E*,*E*-**L** (*i.e.* *Z*-**L** → *E*-**L**). Since lanterns *Z*-**L** and *E*-**L** are similar in size, both lanterns are presumably flexible enough to accommodate both *E*- and *Z*-ligands within the same capsule structure, as has been observed for other capsules containing photoswitchable ligands,[36,37,59] potentially enabling photoswitching to occur within[36,37] the supramolecular frameworks rather than ligand dissociation, switching, and reassociation.[60], ¶ By mixing lanterns *E*-**L** and *Z*-**L** in various ratios, we could generate lanterns with mixed ligand configurations (SI, Section S2.8), although not selectively, resulting in mixtures of species. Nevertheless, these lantern mixtures exhibited comparable ^{1}H NMR signals to those observed during thermal relaxation (SI, Fig. S74), supporting our assumption that the intermediates observed during thermal relaxation could be *Z*,*Z*,*Z*,*E*-**L**, *cis*- and *trans*-*Z*,*Z*,*E*,*E*-**L**, and *Z*,*E*,*E*,*E*-**L**. The computed free energy

differences† among the five states—*Z*,*Z*,*Z*,*Z*-**L** (*Z*-**L**), *Z*,*Z*,*Z*,*E*-**L**, *Z*,*Z*,*E*,*E*-**L**, *Z*,*E*,*E*,*E*-**L**, and *E*,*E*,*E*,*E*-**L** (*E*-**L**) — further solidify this conclusion. These energy differences show a systematic trend, in which each successive ligand change from *E*- to *Z*-configuration increases the relative energy of the given lantern on average by $\Delta G = +48$ kJ mol^{-1}, closely matching the computed *E* → *Z* isomerisation of a free ligand in solution (+47.4 kJ mol^{-1}).

Irradiating lantern *Z*-**L** with 500 nm light causes all ligands to switch back to their respective *E*-configurations, resulting not in the reformation of the 78 : 22 triangle *E*-**T**/lantern *E*-**L** mixture, but in the exclusive formation of lantern *E*-**L** as demonstrated by mass spectrometry, ^{1}H NMR, and DOSY NMR spectroscopy (Fig. 1; SI Section S4.3). The initial 78 : 22 triangle *E*-**T**/lantern *E*-**L** mixture could be regained by equilibrating the sample at 22 °C for at least 8 hours, usually overnight. Furthermore, the light-induced switching and subsequent thermal equilibration could be repeated for five cycles with no appreciable photobleaching (Fig. 3a and S68).

Since 78 : 22 *E*-**T**/*E*-**L** → *Z*-**L** switching under 365 nm light and *Z*-**L** → *E*-**L** switching under 500 nm light are not entirely reversible, resulting in the accumulation of the out-of-equilibrium structure lantern *E*-**L**, we propose, that the switching operates *via* a molecular ratchet mechanism.

A molecular (information) ratchet

To verify the operation of a molecular ratchet mechanism in the *E*-**T**/*E*-**L** → *Z*-**L** and *Z*-**L** → *E*-**L** switching cycle, we investigated both processes *via in situ* illumination ^{1}H NMR spectroscopy (Fig. 3b; SI, Section S4.3).

During 365 nm light irradiation (LED power reduced to 10%), both triangle *E*-**T** and lantern *E*-**L** are converted to lantern *Z*-**L**. After approximately 15 min, the transformation was complete with a PSS of 100% *Z*-**L** and no further changes were observed. Subsequent irradiation with 500 nm light (LED power reduced to 2%) caused the amount of lantern *Z*-**L** to decrease in favour of lantern *E*-**L** rapidly. Lantern *E*-**L**, in turn, instantly begins equilibrating to triangle *E*-**T**, resulting in a maximum population of 11 : 89 triangle *E*-**T**/lantern *E*-**L** after 3 min of 500 nm light irradiation. Lantern *Z*-**L** is entirely consumed after about 10 min of 500 nm light irradiation, after which the gradual equilibration of lantern *E*-**L** to triangle *E*-**T** can be observed. A maximum population of 2 : 98 triangle *E*-**T**/lantern *E*-**L** could be reached upon 500 nm light irradiation by increasing the LED power from 10% to 100% (SI, Fig. S65). In both processes, no half-assembled structures were observed within the detection limits of NMR spectroscopy (SI, Fig. S63 and S64). However, some intermediates could be detected, which we tentatively assign to be the partly switched lantern structures already observed in the thermal relaxation of lantern *Z*-**L**, *i.e.* *Z*,*Z*,*Z*,*E*-**L**, *Z*,*Z*,*E*,*E*-**L**, and *Z*,*E*,*E*,*E*-**L** (see above and SI, Fig. S74). Since these intermediates were minor and could not be clearly identified, we excluded them from the kinetic investigation of the switching cycle.

To further strengthen our hypothesis, that a molecular ratchet mechanism operates within the switching cycle of *E*-**L** + *E*-**T** → *Z*-**L** → *E*-**L** ⇌ *E*-**T** upon iterative irradiation with 365 nm and 500 nm light, we tentatively modelled the kinetics of this intricate process to compare the orders of magnitude of the rate-limiting steps using three independent kinetic models (Scheme 2; SI, Section S5.2).

The kinetic constants of the (rate-determining) steps of the switching cycle obtained by all models support our previous qualitative observations, demonstrating the molecular ratchet mechanism at work (Scheme 2, values of Model III provided; SI, Section S5.2):

(i). Under 365 nm light irradiation, both triangle *E*-**T** and lantern *E*-**L** switch to lantern *Z*-**L** with comparable rate constants ($k_{E\text{-}\mathbf{T}\rightarrow Z\text{-}\mathbf{L}} = 4 \times 10^{-3}$ s^{-1}; $k_{E\text{-}\mathbf{L}\rightarrow Z\text{-}\mathbf{L}} = 5 \times 10^{-3}$ s^{-1}).

(ii). When irradiating lantern *Z*-**L** with 500 nm light, switching and rearranging to lantern *E*-**L** is two orders of magnitude faster than the pathway from lantern *Z*-**L** to triangle *E*-**T**, with $k_{Z\text{-}\mathbf{L}\rightarrow E\text{-}\mathbf{L}} = 10^{-2}$ s^{-1} and $k_{Z\text{-}\mathbf{L}\rightarrow E\text{-}\mathbf{T}} = 8 \times 10^{-4}$ s^{-1}, respectively.

(iii). Reformation of triangle *E*-**T** predominantly occurs *via* the equilibrium between triangle *E*-**T** and lantern *E*-**L**, which is slow at room temperature ($k_{E\text{-}\mathbf{L}\rightarrow E\text{-}\mathbf{T}} = 2 \times 10^{-4}$ s^{-1}).

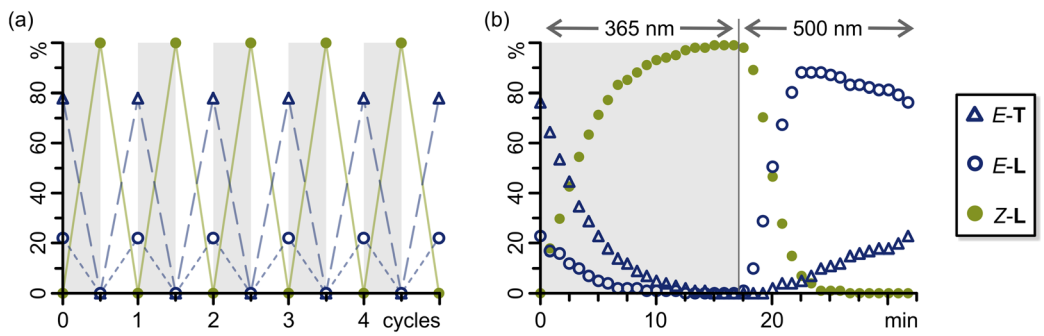

Fig. 3 (a) Investigation of switching reversibility by ^{1}H NMR (500 MHz, DMSO-d_6, 298 K) of triangle *E*-**T**, lantern *E*-**L**, and lantern *Z*-**L**. A 78 : 22 triangle *E*-**T**/lantern *E*-**L** mixture was subjected to alternating light irradiation with 365 nm (5 min) and 500 nm (5 min), respectively. After irradiation with 500 nm light, the sample was left equilibrating for 22 h in an amberised NMR tube wrapped in aluminium foil in an air-conditioned room (22 °C) to allow for equilibration to the 78 : 22 triangle *E*-**T**/lantern *E*-**L** ratio. No apparent photodegradation was observed after five switching cycles. (b) Changes in composition between triangle *E*-**T**, lantern *E*-**L**, and lantern *Z*-**L** measured by *in situ* illumination ^{1}H NMR (700 MHz, DMSO-d_6, 298 K). A sample of 78 : 22 triangle *E*-**T**/lantern *E*-**L** was irradiated with 365 nm light (LED power reduced to 10%) for approx. 17 min to induce *E* → *Z* isomerisation, followed by illumination with 500 nm light (LED power reduced to 2%) for approx. 16 min.

With the kinetic data, we determined the kinetic asymmetry within the molecular ratchet. Under 365 nm irradiation, the kinetic asymmetry for *E*-**T**→*Z*-**L** and *E*-**L**→*Z*-**L** conversions is negligible (0.93 : 1). However, *Z*-**L**→*E*-**T** and *Z*-**L**→*E*-**L** transformations show significant kinetic asymmetry when exposed to 500 nm light (12 : 1; SI, Section S5.3). Since the molecular ratchet is light-driven, increasing the light intensity (from 2% to 100% LED power) also enhances the kinetic asymmetry by a factor of 30, enabling precise control of the molecular ratchet. Hence, this molecular ratchet exploits the kinetic asymmetry in both the thermal and photochemical *Z*-**L** → *E*-**L** and *Z*-**L** → *E*-**T** isomerisations (and subsequent rearrangement) and can therefore be used to accumulate the out-of-equilibrium structure *E*-**L**.

To fully elucidate the thermodynamics of the molecular ratchet, we calculated† the energy difference between lantern *Z*-**L** and lantern *E*-**L** using a model system derived from the crystal structure of lantern *E*-**L**. This model system features the respective lantern with its cavity occupied by four DMSO solvent molecules. Additionally, two BF_4^- anions coordinate to the Pd^{II} cations' octahedral positions outside the lantern (SI, Section S8.6). From this model system, a free-energy difference of $\Delta G = -181.2$ kJ mol^{-1} was obtained. Along with the energy difference between triangle *E*-**T** and lantern *E*-**L** of $\Delta G = -27.8 \pm 13$ kJ mol^{-1} determined *via* Van't Hoff analysis, this completes the thermodynamic picture of the ratchet.

Crucially, the molecular ratchet operates autonomously under continuous white-light irradiation, as minor proportions of both the *E*- and *Z*-states are constantly excited by the white-light spectrum (SI, Fig. S93). We assume white-light irradiation drives the same molecular ratchet reaction cycle as iterative irradiation (Scheme 2), albeit with different kinetic constants. The kinetic asymmetry of the molecular ratchet causes the accumulation of the thermodynamically less stable lantern *E*-**L** (Fig. 4; SI, Section S6). Since the kinetic bias of the molecular ratchet under continuous irradiation depends only on the rate differences of the *Z*-**L** → *E*-**L** and *Z*-**L** → *E*-**T** isomerisations, we classify this as an information ratchet.

White-light irradiation of the 78 : 22 triangle *E*-**T**/lantern *E*-**L** mixture *in situ* in the ^{1}H NMR spectrometer for 5.5 h results in a triangle *E*-**T**/lantern *E*-**L** ratio of 34 : 66, indicating a threefold increase in lantern *E*-**L** population. After leaving the sample at 22 °C in the dark for at least 8 hours, the initial 78 : 22 triangle *E*-**T**/lantern *E*-**L** mixture is restored.

The same threefold increase in lantern *E*-**L** population can be reached by exposing the sample to sunlight for 7 hours, effectively converting sunlight into chemical energy. In terms of energy, consecutive irradiation with 365 nm and 500 nm light stores 21.1 kJ mol^{-1} of light as chemical energy within the system, whereas the continuous operation of the information ratchet with white light stores 12.2 kJ mol^{-1}. These values translate to energy storage efficiencies of 0.04% and 3×10^{-5}%, respectively (SI, Section S5.4). Thus, under iterative irradiation, our system exceeds the energy storage of previously reported fuel-[61,62] or photochemically driven[63,64] systems with comparable first-cycle efficiency.[61–64] While continuous operation of the information ratchet under white light is less efficient, this drawback can be fully offset by using direct sunlight—which is both abundant and free—to drive the ratchet.[65] Furthermore, compared to fuel-driven systems, our light-driven system does not suffer from diminished effectiveness due to waste accumulation,[61,62,66] instead exhibiting excellent fatigue resistance (SI, Fig. S57).

Therefore, our system demonstrates the direct conversion and storage of sunlight as chemical energy in a thermodynamically disequilibrated system.

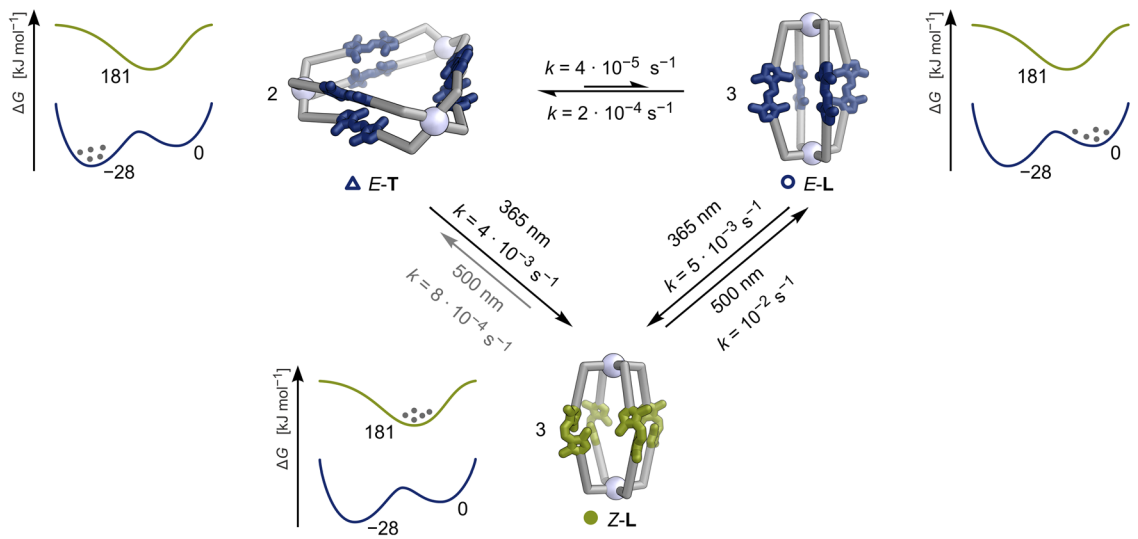

Scheme 2 Schematic representation of the molecular ratchet governing the triangle *E*-T/lantern *E*-L → lantern *Z*-L switching cycle upon iterative irradiation with 365 nm and 500 nm light. The rate constants of the respective steps obtained from one of the kinetic models were determined in three separate experiments and are indicated alongside the reaction arrows (SI, Section S5.2, for detailed description of the kinetic model). Next to each state, a schematic diagram of the potential energy surface and its population is illustrated along with the respective energies — either experimental or computed — of the three states (*Z*-states: blue; *E*-states: green).

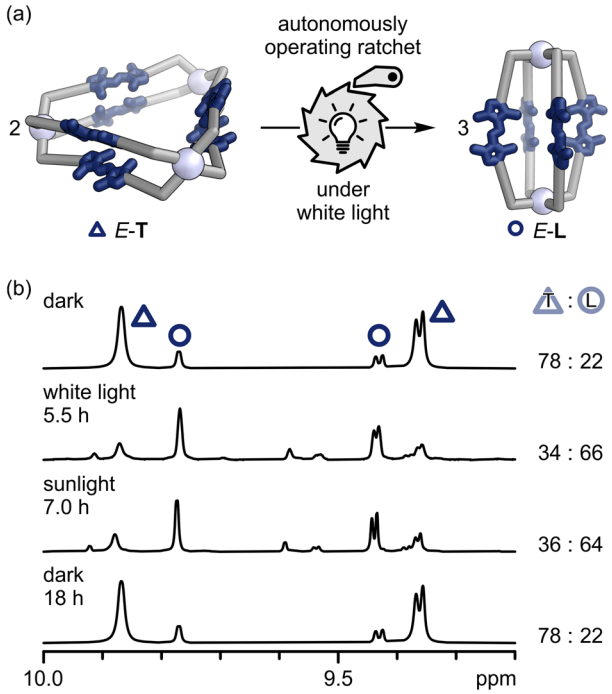

Fig. 4 (a) Continuous exposure to white light powers the ratchet autonomously, leading to the formation of lantern *E*-**L**. We assume white-light irradiation drives the same molecular ratchet cycle as iterative irradiation (Scheme 2), but with different kinetics. (b) ^{1}H NMR spectra (700 MHz, DMSO-d_6, 298 K) of the 78 : 22 triangle *E*-**T**/lantern *E*-**L** mixture under light exclusion, after *in situ* illumination with white light for 5.5 h (*E*-**T**/*E*-**L** 34 : 66), after exposing the sample to sunlight on a sunny spring day for 7 h (*E*-**T**/*E*-**L** 36 : 64), and after equilibrating the sample under light exclusion at 22 °C for 22 h (*E*-**T**/*E*-**L** 78 : 22; top to bottom).

Conclusion

In summary, azobispyrazol-based ligand **1** is an excellent photoswitch, exhibiting near-quantitative $E \rightarrow Z$ and $Z \rightarrow E$ conversions. Due to the conformational flexibility provided by the five-membered pyrazole rings, the ligand can adopt two conformations with coordination-vector bite angles of 0° and 60°, respectively, which both lead to metallo-supramolecular architectures: a double-walled triangle *E*-**T** and a lantern *E*-**L**. Since these structures require different ligand coordination vector bite angles (60° and 0°, respectively), they are usually not accessible from the same ligand structure.

Photoswitching of the equilibrated 78 : 22 triangle *E*-**T**/lantern *E*-**L** mixture occurs *via* a molecular ratchet mechanism, which we have elucidated in terms of both kinetics and thermodynamics, with the aid of quantum chemistry-based calculations: irradiation with 365 nm light affords lantern *Z*-**L** exclusively, which then switches back to out-of-equilibrium lantern *E*-**L** exclusively. Triangle *E*-**T** subsequently forms from lantern *E*-**L** through thermodynamic equilibration.

Crucially, the molecular ratchet operates autonomously under white light, effectively converting sunlight into an out-of-equilibrium structure, *i.e.* chemical energy, and temporarily storing it.

This work proves that autonomous, light-driven processes can be effectively harnessed to precisely control non-equilibrium behaviour in complex coordination assemblies.

Author contributions

L. P. L.: synthesis, characterisation, photoswitching studies. B. B.: computational studies. M. J. N.: fitting of kinetic data and their interpretation, calculation of energy storage. G. S.: X-ray crystallography. S. G.: supervision. L. K. S. v. K.: project conception and supervision. The manuscript was written through contributions of all authors. All authors have given approval to the final version of the manuscript.

Conflicts of interest

There are no conflicts to declare.

Data availability

CCDC 2488074 (*E*-**1**) and 2488075 (*E*-**L**) contain the supplementary crystallographic data for this paper.[94a,b]

The authors have cited additional references within the supplementary information (SI).[67–90] Additionally, *xyz* coordinates of computed structures are provided (zip). Supplementary information: detailed experimental and characterisation data including NMR and mass spectra; X-ray crystallographic information; additional details of computational structure simulations. See DOI: https://doi.org/10.1039/d5sc09472k.

Acknowledgements

This work is supported by the Fonds der Chemischen Industrie (FCI, Liebig Fellowship) and the German Research Foundation (DFG; Emmy Noether Programme, 446317932). L. P. L. thanks U. Weynand and Dr. S. Nozinovic for support with NMR measurements. M. J. N. and L. K. S. v. K. thank Dr B. M. W. Roberts and Dr. R. J. Mayer for the helpful discussions regarding the fitting of kinetic data. B. B. and S. G. gratefully acknowledge the access to the Marvin cluster of the University of Bonn. G. S. thanks Prof. Dr. A. C. Filippou for providing X-ray infrastructure.

Notes and references

† All computed lantern structures were conformationally sampled using the CREST[56] program at the GFN2-xTB [ALPB: DMSO][46,47] level of theory. Using the ORCA software package,[86] the lowest conformers were optimised at the ωB97X-3c [CPCM: DMSO][57,72] level of theory, while the SMD[90] model was used for the final single-point calculations. Thermal corrections were computed at the GFN2-xTB [ALPB: DMSO] level of theory employing the mRRHO approximation,[85] using the xTB software package.[74,85,91]

‡ The different capsule isomers are reminiscent of those in amide-linked organic capsules.[92,93]

§ Although *Z*-**1** is chiral and *Z*-**L** exists as a mixture of diastereomers, only minor shifts and no signal splitting were observed upon addition of the chiral shifting reagent Δ-TRISPHAT (SI, Fig. S27). This suggests that the diastereomers are likely the two *meso* forms or that their interaction with Δ-TRISPHAT occurs on fast exchange on the NMR timescale.

¶ Note that the rates of photoswitching *versus* capsule rearrangement, as determined by kinetic Model I (SI, Section S5.2.1), might support the hypothesis that photoswitching occurs within the supramolecular frameworks rather than through ligand dissociation, switching, and reassociation.

1 T. Sangchai, S. A. Shehimy, E. Penocchio and G. Ragazzon, *Angew. Chem., Int. Ed.*, 2023, **62**, e202309501.
2 S. Borsley, D. A. Leigh and B. M. W. Roberts, *Angew. Chem., Int. Ed.*, 2024, **63**, e202400495.
3 R. D. Astumian, *Acc. Chem. Res.*, 2018, **51**, 2653–2661.
4 A. W. Heard and S. M. Goldup, *ACS Cent. Sci.*, 2020, **6**, 117–128.
5 E. R. Kay, D. A. Leigh and F. Zerbetto, *Angew. Chem., Int. Ed.*, 2006, **46**, 72–191.
6 M. Kathan, S. Crespi, N. O. Thiel, D. L. Stares, D. Morsa, J. de Boer, G. Pacella, T. van den Enk, P. Kobauri, G. Portale, C. A. Schalley and B. L. Feringa, *Nat. Nanotechnol.*, 2022, **17**, 159–165.
7 R. D. Astumian and I. Derényi, *Eur. Biophys. J.*, 1998, **27**, 474–489.
8 M. Kathan, F. Eisenreich, C. Jurissek, A. Dallmann, J. Gurke and S. Hecht, *Nat. Chem.*, 2018, **10**, 1031–1036.
9 K. Das, L. Gabrielli and L. J. Prins, *Angew. Chem., Int. Ed.*, 2021, **60**, 20120–20143.
10 M. Alvarez-Pérez, S. M. Goldup, D. A. Leigh and A. M. Z. Slawin, *J. Am. Chem. Soc.*, 2008, **130**, 1836–1838.
11 V. Serreli, C.-F. Lee, E. R. Kay and D. A. Leigh, *Nature*, 2007, **445**, 523–527.
12 R. E. Spinney, M. Prokopenko and D. Chu, *Phys. Rev. E*, 2018, **98**, 022124.
13 E. Liu, S. Cherraben, L. Boulo, C. Troufflard, B. Hasenknopf, G. Vives and M. Sollogoub, *Chem*, 2023, **9**, 1147–1163.
14 E. Liu, D. Daou, B. Hasenknopf, G. Vives and M. Sollogoub, *Chem*, 2025, 102623.
15 J. A. Berrocal, C. Biagini, L. Mandolini and S. D. Stefano, *Angew. Chem., Int. Ed.*, 2016, **55**, 6997–7001.
16 S. Erbas-Cakmak, S. D. P. Fielden, U. Karaca, D. A. Leigh, C. T. McTernan, D. J. Tetlow and M. R. Wilson, *Science*, 2017, **358**, 340–343.
17 S. Erbas-Cakmak, D. A. Leigh, C. T. McTernan and A. L. Nussbaumer, *Chem. Rev.*, 2015, **115**, 10081–10206.
18 M. A. Watson and S. L. Cockroft, *Chem. Soc. Rev.*, 2016, **45**, 6118–6129.
19 G. Ragazzon, M. Malferrari, A. Arduini, A. Secchi, S. Rapino, S. Silvi and A. Credi, *Angew. Chem., Int. Ed.*, 2023, **62**, e202214265.
20 S. J. Wezenberg, *Chem. Commun.*, 2022, **58**, 11045–11058.
21 D.-H. Qu, Q.-C. Wang, Q.-W. Zhang, X. Ma and H. Tian, *Chem. Rev.*, 2015, **115**, 7543–7588.
22 R. G. DiNardi, A. O. Douglas, R. Tian, J. R. Price, M. Tajik, W. A. Donald and J. E. Beves, *Angew. Chem., Int. Ed.*, 2022, **61**, e202205701.
23 R. G. DiNardi, S. Rasheed, S. S. Capomolla, M. H. Chak, I. A. Middleton, L. K. Macreadie, J. P. Violi, W. A. Donald, P. J. Lusby and J. E. Beves, *J. Am. Chem. Soc.*, 2024, **146**, 21196–21202.
24 M. Ovalle, M. Kathan, R. Toyoda, C. N. Stindt, S. Crespi and B. L. Feringa, *Angew. Chem., Int. Ed.*, 2023, **62**, e202214495.
25 R. I. Petrikat, J. Hornbogen, M. J. P. Schmitt, E. Resmann, C. Wiedemann, N. I. Dilmen, H. Schneider, A. M. Pick, C. Riehn, R. Diller and S. Becker, *Chem. Eur. J.*, 2024, **30**, e202400205.
26 J. Gemen, J. R. Church, T.-P. Ruoko, N. Durandin, M. J. Białek, M. Weißenfels, M. Feller, M. Kazes, M. Odaybat, V. A. Borin, R. Kalepu, Y. Diskin-Posner, D. Oron, M. J. Fuchter, A. Priimagi, I. Schapiro and R. Klajn, *Science*, 2023, **381**, 1357–1363.
27 I. Neira, C. Taticchi, F. Nicoli, M. Curcio, M. D. Garcia, C. Peinador, S. Silvi, M. Baroncini and A. Credi, *Chem*, 2025, **11**, 102375.
28 D. Hugenbusch, M. Lehr, J. von Glasenapp, A. J. McConnell and R. Herges, *Angew. Chem., Int. Ed.*, 2023, **62**, e202212571.
29 H. Lee, J. Tessarolo, D. Langbehn, A. Baksi, R. Herges and G. H. Clever, *J. Am. Chem. Soc.*, 2022, **144**, 3099–3105.
30 M. J. Notheis, G. Schnakenburg and L. K. S. von Krbek, *Angew. Chem., Int. Ed.*, 2025, e202508952.
31 C. Stuckhardt, D. Roke, W. Danowski, E. Otten, S. J. Wezenberg and B. L. Feringa, *Beilstein J. Org. Chem.*, 2019, **15**, 2767–2773.
32 D. Villarón and S. J. Wezenberg, *Angew. Chem., Int. Ed.*, 2020, **59**, 13192–13202.
33 J. Wu and J. L. Greenfield, *Chem*, 2025, 102579.
34 J. Wu, L. Kreimendahl and J. L. Greenfield, *Angew. Chem., Int. Ed.*, 2025, **64**, e202415464.
35 M. Han, R. Michel, B. He, Y. Chen, D. Stalke, M. John and G. H. Clever, *Angew. Chem., Int. Ed.*, 2013, **52**, 1319–1323.
36 R. Li, M. Han, J. Tessarolo, J. J. Holstein, J. Lübben, B. Dittrich, C. Volkmann, M. Finze, C. Jenne and G. H. Clever, *ChemPhotoChem*, 2019, **3**, 378–383.
37 R.-J. Li, J. J. Holstein, W. G. Hiller, J. Andréasson and G. H. Clever, *J. Am. Chem. Soc.*, 2019, **141**, 2097–2103.
38 A. Carbonell, I. Izquierdo, D. B. G. Ríos, G. Norjmaa, G. Ujaque, A. J. Martínez-Martínez and U. Pischel, *Inorg. Chem.*, 2024, **63**, 19872–19884.
39 E. Benchimol, J. Tessarolo and G. H. Clever, *Nat. Chem.*, 2024, **16**, 13–21.
40 A. D. W. Kennedy, R. G. DiNardi, L. L. Fillbrook, W. A. Donald and J. E. Beves, *Chem. Eur J.*, 2022, **28**, e202104461.
41 S. Millan, J. Nasir, B. Gil-Hernández, T.-O. Knedel, B. Moll, I. Boldog, O. Weingart, J. S. auf der Günne and C. Janiak, *Cryst. Growth Des.*, 2020, **20**, 2721–2733.
42 A. Gonzalez, M. Odaybat, M. Le, J. L. Greenfield, A. J. P. White, X. Li, M. J. Fuchter and G. G. D. Han, *J. Am. Chem. Soc.*, 2022, **144**, 19430–19436.
43 Y. He, Z. Shangguan, Z. Zhang, M. Xie, C. Yu and T. Li, *Angew. Chem., Int. Ed.*, 2021, **60**, 16539–16546.
44 Y. He, T. Dang, A. G. Leach, Z.-Y. Zhang and T. Li, *J. Am. Chem. Soc.*, 2024, **146**, 29237–29244.
45 S. Millan, B. Gil-Hernández, E. Hastürk, A. Schmitz, C. Janiak and Z. für, *Z. Anorg. Allg. Chem.*, 2018, **644**, 1311–1316.
46 S. Ehlert, M. Stahn, S. Spicher and S. Grimme, *J. Chem. Theory Comput.*, 2021, **17**, 4250–4261.
47 C. Bannwarth, S. Ehlert and S. Grimme, *J. Chem. Theory Comput.*, 2019, **15**, 1652–1671.

48 D. Pirone, N. A. G. Bandeira, B. Tylkowski, E. Boswell, R. Labeque, R. G. Valls and M. Giamberini, *Polymers*, 2020, **12**, 1019.
49 S. S. Mishra, S. Krishnaswamy and D. K. Chand, *J. Am. Chem. Soc.*, 2024, **146**, 4473–4488.
50 S. M. Jansze and K. Severin, *J. Am. Chem. Soc.*, 2019, **141**, 815–819.
51 G. H. Clever and P. Punt, *Acc. Chem. Res.*, 2017, **50**, 2233–2243.
52 M. R. Black, S. Bhattacharyya, S. P. Argent and B. S. Pilgrim, *J. Am. Chem. Soc.*, 2024, **146**, 28233–28241.
53 R. G. DiNardi, A. O. Douglas, R. Tian, J. R. Price, M. Tajik, W. A. Donald and J. E. Beves, *Angew. Chem., Int. Ed.*, 2022, **61**, e202205701.
54 J. Harada and K. Ogawa, *Chem. Soc. Rev.*, 2009, **38**, 2244–2252.
55 W. Moormann, T. Tellkamp, E. Stadler, F. Röhricht, C. Näther, R. Puttreddy, K. Rissanen, G. Gescheidt and R. Herges, *Angew. Chem., Int. Ed.*, 2020, **59**, 15081–15086.
56 P. Pracht, S. Grimme, C. Bannwarth, F. Bohle, S. Ehlert, G. Feldmann, J. Gorges, M. Müller, T. Neudecker, C. Plett, S. Spicher, P. Steinbach, P. A. Wesołowski and F. Zeller, *J. Chem. Phys.*, 2024, **160**, 114110.
57 M. Müller, A. Hansen and S. Grimme, *J. Chem. Phys.*, 2023, **158**, 014103.
58 P. Pracht, *J. Chem. Inf. Model.*, 2025, **65**, 4501–4511.
59 M. B. Tipping, L. Pruñonosa Lara, A. B. Solea, L. K. S. von Krbek and M. D. Ward, *Chem. Sci.*, 2024, **15**, 8488–8499.
60 A. D. W. Kennedy, R. G. DiNardi, L. L. Fillbrook, W. A. Donald and J. E. Beves, *Chem. Eur. J.*, 2022, **28**, e202104461.
61 E. Olivieri, J. M. Gallagher, A. Betts, T. W. Mrad and D. A. Leigh, *Nat. Synth.*, 2024, **3**, 707–714.
62 S. A. Shehimy, H. Le, S. Amano, S. D. Noja, L. Monari and G. Ragazzon, *Angew. Chem., Int. Ed.*, 2024, **63**, e202411554.
63 A. Hölzl-Hobmeier, A. Bauer, A. V. Silva, S. M. Huber, C. Bannwarth and T. Bach, *Nature*, 2018, **564**, 240–243.
64 N. Y. Shin, J. M. Ryss, X. Zhang, S. J. Miller and R. R. Knowles, *Science*, 2019, **366**, 364–369.
65 H. Wang, Y.-M. Tian and B. König, *Nat. Rev. Chem.*, 2022, **6**, 745–755.
66 S. Borsley, J. M. Gallagher, D. A. Leigh and B. M. W. Roberts, *Nat. Rev. Chem.*, 2024, **8**, 8–29.
67 S. Takahashi, Y. Sasaki, S. Hiraoka and H. Sato, *Phys. Chem. Chem. Phys.*, 2018, **21**, 6341–6347.
68 M. D. Hanwell, D. E. Curtis, D. C. Lonie, T. Vandermeersch, E. Zurek and G. R. Hutchison, *J. Cheminform.*, 2012, **4**, 17.
69 P. V. D. Sluis and A. L. Spek, *Acta Crystallogr., Sect. A*, 1990, **46**, 194–201.
70 H. Hoops, S. Sahle, R. Gauges, C. Lee, J. Pahle, N. Simus, M. Singhal, L. Xu, P. Mendes and U. Kummer, *Bioinformatics*, 2006, **22**, 3067–3074.
71 G. M. Sheldrick, *Acta Crystallogr., Sect. C: Struct. Chem.*, 2015, **71**, 3–8.
72 M. Cossi, N. Rega, G. Scalmani and V. Barone, *J. Comput. Chem.*, 2003, **24**, 669–681.
73 S. Grimme, *J. Chem. Theory Comput.*, 2019, **15**, 2847–2862.
74 C. Bannwarth, E. Caldeweyher, S. Ehlert, A. Hansen, P. Pracht, J. Seibert, S. Spicher and S. Grimme, *Wiley Interdiscip. Rev.: Comput. Mol. Sci.*, 2020, **11**(2), DOI: 10.1002/wcms.1493.
75 C. Feldmeier, H. Bartling, E. Riedle and R. M. Gschwind, *J. Magn. Reson.*, 2013, **232**, 39–44.
76 Y. Ji, D. A. DiRocco, J. Kind, C. M. Thiele, R. M. Gschwind and M. Reibarkh, *ChemPhotoChem*, 2019, **3**, 984–992.
77 T. Tateishi, T. Kojima and S. Hiraoka, *Inorg. Chem.*, 2018, **57**, 2686–2694.
78 T. Tateishi, S. Takahashi, A. Okazawa, V. Martí-Centelles, J. Wang, T. Kojima, P. J. Lusby, H. Sato and S. Hiraoka, *J. Am. Chem. Soc.*, 2019, **141**, 19669–19676.
79 O. V. Dolomanov, L. J. Bourhis, R. J. Gildea, J. A. K. Howard and H. Puschmann, *J. Appl. Crystallogr.*, 2009, **42**, 339–341.
80 M. S. Maier, K. Hüll, M. Reynders, B. S. Matsuura, P. Leippe, T. Ko, L. Schäffer and D. Trauner, *J. Am. Chem. Soc.*, 2019, **141**, 17295–17304.
81 S. Grimme, A. Hansen, S. Ehlert and J.-M. Mewes, *J. Chem. Phys.*, 2021, **154**, 064103.
82 B. A. Inc., SADABS-2016/2, Madison, Wisconsin, USA, 2016.
83 S. Kai, T. Tateishi, T. Kojima, S. Takahashi and S. Hiraoka, *Inorg. Chem.*, 2018, **57**, 13083–13086.
84 G. M. Sheldrick, *Acta Crystallogr., Sect. A*, 2015, **71**, 3–8.
85 S. Spicher and S. Grimme, *J. Chem. Theory Comput.*, 2021, **17**, 1701–1714.
86 F. Neese, *Wiley Interdiscip. Rev.: Comput. Mol. Sci.*, 2022, **12**(5), DOI: 10.1002/wcms.1606.
87 S. Ghosh, C. Eschen, N. Eleya and A. Staubitz, *J. Org. Chem.*, 2023, **88**, 3372–3377.
88 T. Tateishi, S. Kai, Y. Sasaki, T. Kojima, S. Takahashi and S. Hiraoka, *Chem. Commun.*, 2018, **54**, 7758–7761.
89 E. F. Pettersen, T. D. Goddard, C. C. Huang, E. C. Meng, G. S. Couch, T. I. Croll, J. H. Morris and T. E. Ferrin, *Protein Sci.*, 2021, **30**, 70–82.
90 A. V. Marenich, C. J. Cramer and D. G. Truhlar, *J. Phys. Chem. B*, 2009, **113**, 6378–6396.
91 GitHub - grimme-lab/xtb: Semiempirical Extended Tight-Binding Program Package, https://github.com/grimme-lab/xtb, (accessed 12 August 2025).
92 K. G. Andrews, P. N. Horton and S. J. Coles, *Chem. Sci.*, 2024, **15**, 6536–6543.
93 C. E. Shields, T. Fellowes, A. G. Slater, A. I. Cooper, K. G. Andrews and F. T. Szczypiński, *Chem. Commun.*, 2024, **60**, 6023–6026.
94 (*a*) CCDC 2488074: Experimental Crystal Structure Determination, 2026, DOI: 10.5517/ccdc.csd.cc2pj1gr; (*b*) CCDC 2488075: Experimental Crystal Structure Determination, 2026, DOI: 10.5517/ccdc.csd.cc2pj1hs.